CrossMark

MAGNETIC RESONANCE

Dynamic contrast enhanced MR imaging for evaluation of angiogenesis of hepatocellular nodules in liver cirrhosis in N-nitrosodiethylamine induced rat model

Wei Zhang[1] · Hui Juan Chen[1] · Zhen J. Wang[2] · Wei Huang[1] · Long Jiang Zhang[1]

Abstract

Purpose To investigate whether dynamic contrast -enhanced MRI (DCE-MRI) can distinguish the type of liver nodules in a rat model with N-nitrosodiethylamine- induced cirrhosis.

Methods Liver nodules in cirrhosis were induced in 60 male Wistar rats via 0.01 % N-nitrosodiethylamine in the drinking water for 35-100 days. The nodules were divided into three groups: regenerative nodule (RN), dysplastic nodule (DN), and hepatocellular carcinoma (HCC). DCE-MRI was performed, and parameters including transfer constant (K^{trans}), rate constant (K_{ep}), extravascular extracellular space volume fraction (V_e), and initial area under the contrast concentration versus time curve (iAUC) were measured and compared.

Results The highest K^{trans} and iAUC values were seen in HCC, followed by DN and RN (all $P < 0.05$). The area under the receiver operating characteristic curve (AUROC) for DN and HCC were 0.738 and 0.728 for K^{trans} and iAUC, respectively. The AUROC for HCC were 0.850 and 0.840 for K^{trans} and iAUC, respectively. Ordinal logistic regression analysis showed that K^{trans} had a high goodness of fit (0.970, 95 % confidence interval, 13.751-24.958).

Conclusion DCE-MRI is a promising method to differentiate of liver nodules. Elevated K^{trans} suggested that the nodules may be transformed into HCC.

Key points
• *DCE-MRI is promising for differentiating among RN, DN, and HCC*
• *K^{trans} and iAUC positively correlated with malignancy degree of liver nodules*
• *Elevated K^{trans} suggests that the nodules may be transformed into HCC*

Abbreviations

DCE-MRI	dynamic contrast- enhanced MRI
K^{trans}	transfer constant
K_{ep}	rate constant
V_e	extravascular extracellular volume fraction
iAUC	initial area under the gadolinium concentration-time curve
AUROC	area under the receiver operating characteristic curve
RN	regenerative nodule
DN	dysplastic nodule
HCC	hepatocellular carcinoma

✉ Wei Huang
radiology@126.com

✉ Long Jiang Zhang
kevinzhlj@163.com

1 Department of Medical Imaging, Jinling Hospital, Medical School of Nanjing University, Nanjing, Jiangsu 210002, China

2 Department of Radiology and Biomedical Imaging, University of California, San Francisco, CA, USA

Introduction

Hepatocellular carcinoma (HCC) is the fifth most prevalent cancer and the third most frequent cause of cancer-related death [1, 2]. Approximately 80 % of HCC develops in patients

with a cirrhotic liver. In addition, HCC is the most common cause of death in patients with cirrhosis [3, 4]. The transformation from regenerative nodules (RN) to HCC is a complex, multistep process. The International Working Party of the World Congresses of Gastroenterology classified nodular lesions found in chronic liver disease into RN, low-grade dysplastic nodule (LGDN), high-grade dysplastic nodule (HGDN), and HCC. Among them, DN is a precancerous lesion [5]. The prognosis of HCC depends largely on the stage at which the tumour is detected. However, patients with early HCCs usually do not have symptoms. In most cases when the symptoms such as abdominal pain, abdominal distension, loss of appetite, and emaciation appear, the disease is already advanced. Some recent studies have shown that nodules found in patients with chronic liver disease or history of hepatocellular nodules may turn into hepatocellular carcinoma in a short time [6, 7]. Therefore, it is critical to monitor the development of hepatocellular nodules in patients with cirrhosis in order to institute appropriate treatment and to improve prognosis.

In recent years, many studies have suggested that angiogenesis is implicated in the transformation of cirrhotic nodules to HCC [8–11]. As the liver nodules become more malignant, the intranodular portal venous blood supply decreases, and the intranodular arterial blood supply initially decreases slightly and subsequently increases rapidly. In other words, malignant nodules have increased unpaired arteries [8, 9]. Parket et al [10] studied 122 nodules and concluded that unpaired arteries were rare in RN, significantly more common in DN, and the most common in HCC. The International Consensus Group for Hepatocellular Neoplasia (ICGHN) also pointed out that the number of unpaired arteries had a role in the differential diagnosis of DN and early HCC [5]. There appears to be a close correlation between the change of the microvasculature and pathological classification in nodules in cirrhosis.

Fine needle aspiration biopsy and immunohistochemical staining for measuring microvessel density (MVD) is the "gold standard" for diagnosing nodules in liver cirrhosis and judging the angiogenesis status. However, it is not suitable for long-term monitoring and assessing therapeutic response due to its invasiveness, costs, and sampling variability. Imaging techniques, especially contrast-enhanced CT and MR imaging have been used to provide quantitative assessment of tumour vasculature, and have the potential to differentiate noninvasively the various nodules in cirrhosis.

Dynamic contrast -enhanced magnetic resonance imaging (DCE-MRI) consists of continuous acquisition of images before, during, and after the injection of contrast agent. Using this technique, several quantitative parameters including transfer constant (K^{trans}), rate constant (K_{ep}), extravascular extracellular space volume fraction (V_e), and semi-quantitative parameters such as the initial area under the gadolinium concentration-time curve (iAUC) can be measured [12–15]. These parameters can evaluate microcirculation perfusion statues of tissues such as vascular perfusion, permeability, and tissue volume fractions noninvasively. DCE-MRI has been used in several thousand studies since the mid - 1990's to diagnose disease, target biopsy, and to evaluate response to therapy [16–28]. To our knowledge, there is no study focusing on microvascular change in the transformation of cirrhotic nodules to HCC using DCE-MRI. Therefore, the purpose of this study was to investigate whether DCE-MRI can monitor the process of microvascular reconstruction in cirrhotic nodules and to provide early diagnosis of HCC.

## Materials and methods

Animal model

This study was approved by the institutional animal care and use committee of (Jinling Hospital, Medical School of Nanjing University, Nanjing, China) and was performed in accordance with institutional guidelines. Sixty adult male Wistar rats (Laboratory Animal Centre of Academy of Military Medical Sciences, Beijing, China), initially weighing 150–170 g, were housed in conventional cages with free access to standard laboratory food and kept at a room temperature of 20-22 °C with a 12-h light-dark cycle. Liver nodules were induced by 0.01 % N-nitrosodiethylamine added to drinking water (0.95 g/L, Sigma-Aldrich, USA) for 35-100 days.

DCE MR imaging

From the fifth week (35th day) on, two to four rats were examined in a 3 Tesla MR scanner (Magnetron Trio; Siemens Medical Solutions, Erlangen, Germany) using a custom-built animal coil (Siemens) every 7 days (Fig. 1). To reduce the artefacts from distended stomach and intestine, rats were fasted for 8 to 12 h before MR scans. All scans were performed under general anaesthesia, which was started in an induction chamber using a mixture of 4 % isoflurane (Keyuan Pharmaceutical Co., Jinan, China) and 96 % oxygen, and then maintained with an animal nose mask supplying a mixture of 2 % isoflurane and 98 % oxygen at a flow rate of 0.8 L/min. In order to reduce respiratory movement, each rat's abdomen was wrapped with gauze before being positioned prone in the animal coil.

The precontrast scans for locating nodules included coronal T_2 weighted imaging (T_2WI), axial T_1 weighted imaging (T_1WI), and axial T_2 weighted imaging (T_2WI), and all were performed with a turbo spin echo (TSE) sequence. For the coronal T_2WI, the images were acquired with repetition time (TR)/echo time (TE) of 4000 ms/68 ms, flip angle (FA) of 160°, field of view (FOV) of 100×100 mm^2, and slice thickness of 2.5 mm with 0.25 mm gap. For the axial T_1WI, the images were acquired with TR/ TE of 805 ms/13 ms, FA of 150°, FOV of 53×53 mm^2 , and slice thickness of 2.5 mm/

Fig. 1 The flow chart of the experiment. At the 100th day (15th week), administration of N-nitrosodiethylamine was stopped. The first scan was at the 35th day (end of 5th week) after the administration of N-Nnitrosodiethylamine. Nineteen rats died due to HCC and related complications such as tumour rupture during the experiment. Another two rats died due to poor tolerance to anaesthesia at the 13th and 15th week (*) during MR scan. Week X = time after administration of N-nitrosodiethylamine RN = regenerative nodule, DN = dysplastic nodule, HCC = hepatocellular carcinoma, K^{trans} = transfer constant, K_{ep} = rate constant, V_e = extravascular extracellular volume fraction; iAUC = initial area under the gadolinium concentration-time curve
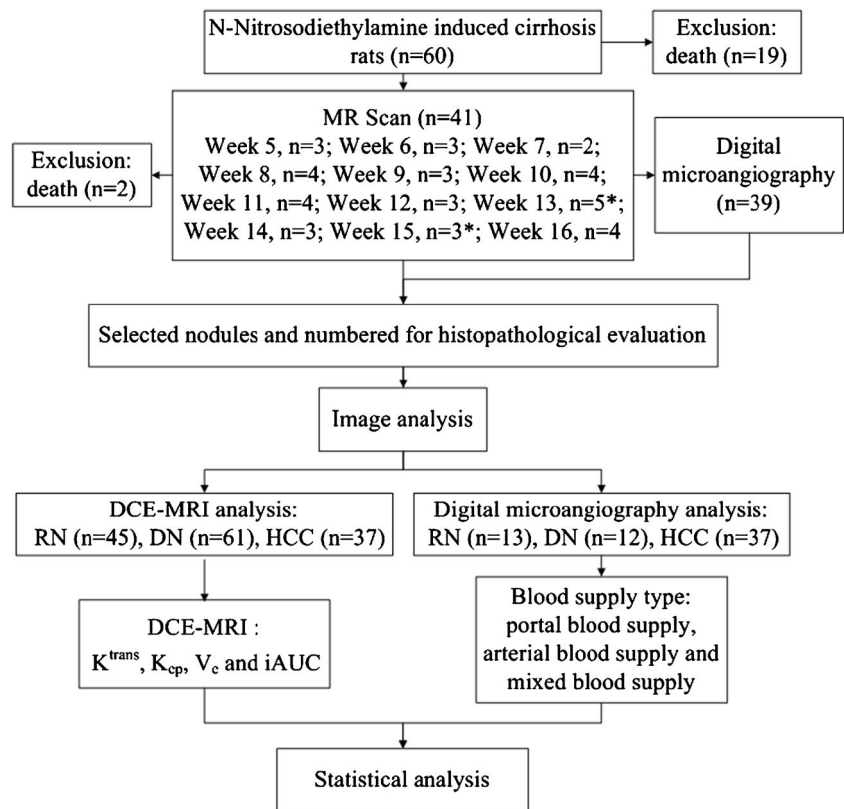
0.25 mm gap. For the axial T_2WI, the images were acquired with TR/ TE of 3000 ms/57 ms, FA of 140°, FOV of 100×100 mm^2, and slice thickness of 2.5 mm/0.25 mm gap. The DCE-MRI data were acquired using free-breathing three-dimensional volumetric interpolated breath-hold examination (3D-VIBE) sequences with the following parameters: TR/ TE = 7.74 ms/2.32 ms, FA = 12°, FOV = 70×50.75 mm^2, matrix size = 192×138. The scanning process contained 60 continuous measurements lasting for 10 min 27 s, and each measurement had 16 axial slices with thickness of 1.5 mm and slice gap of 0.3 mm [14]. At the end of the third measurement, 0.2 mmol/kg (0.8 ml/kg) 50 % Gd-DTPA (Magnevist, Beijing BeiLu Pharmaceutical Co., Ltd, Beijing, China) was injected through a previously inserted tail vein catheter (24G, BD, Suzhou, China) by hand, followed by a 1 mL saline flush [14, 29]. Before the DCE-MRI acquisition, images for calculating T_1 maps were acquired using the same sequence and parameters except for the flip angle (2° and 15°) [14].

Digital microangiography

Immediately after the last MRI session, laparotomy was performed. Abdominal aorta and portal vein were cannulated for digital microangiography. After that, rats were euthanized with an intravenous overdose of chloral hydrate. To determine the source of blood supply to the nodules, barium suspension (Qingdao Dongfeng chemical co., LTD, Qingdao, China) was

first injected through the abdominal aorta until the appearance of barium in distal capillaries. Using a GIOTTO Mammography Unit (IMS Internazionale Medico Scientifica S.R.L., Italy) at 25 kV and 6 mAs, hepatic arteriography was made [30]. After that, barium suspension was injected through the portal vein until the barium flow out from the posterior vena cava, and hepatic portography was performed.

Cirrhotic nodule numbers

After digital microangiography, liver specimen was fixed in $4.2 \sim 5.2$ % formaldehyde neutral buffer solution for 2 h. When fixing the liver, a hemostat was used to clamp the vena cava in order to hang it over the formaldehyde neutral buffer solution in order to fix the liver in similar anatomical location. Then, the livers were cut into slices with the same thickness as the axial MRI sequence. Liver nodules were located in axial T_1W, T_2W, DCE-MRI, and coronal T_2W images. The nodules that could be accurately positioned were removed and numbered for the calculation of DCE-MRI parameters. The nodules that could be accurately positioned with microangiography in a non-overlapping position were also numbered for the observation of blood supply.

Imaging analysis

DCE-MRI parameters including K^{trans}, K_{ep}, V_e, and iAUC of the numbered nodules were measured from DCE-MR images

using a commercial post-processing software based on a two-compartment Tofts model (Tissue 4D, Siemens Medical Solutions) installed at an image processing workstation (Syngo MMWP, Siemens Medical Solutions). The arterial input function (AIF) was measured at the abdominal aorta and the venous input function (VIF) was measured at the main portal vein. Because the default option of Tissue 4D was AIF, all DCE-MRI parameters of cirrhotic nodules were calculated by AIF. Regions of interest (ROI) were drawn by hand in the maximal section of nodules. Care was taken to avoid large vessels, cystic or necrotic regions, and regions with severe motion artefact. All the DEC-MRI parameters of each nodule were measured three times and their average values were used in the final analysis. Averaging was performed in order to reduce the effect of differences in the selected areas of interest (ROIs), and thus measurement values between different observers.

Histopathological and immunohistochemical evaluation

In order to determine the nature of the nodules, the fixed nodules were dehydrated, embedded in paraffin, cut in 5 μm sections and mounted on the slide. The haematoxylin-eosin (HE) stain was used for histopathological examination. All nodules were histologically diagnosed according to the recommendation of the International Working Party (1995) and divided into three groups: RN, DN, and HCC. Liver slices were also used for CD31 staining. The CD31 staining was performed by the avidin-biotin-peroxidase complex method, with the antibody PECAM-1 (M-20) (sc-1506, Santa Cruz Biotechnology, INC., USA).

Statistical analysis

Statistical analysis was performed by using the IBM SPSS Statistics 20 software. Data were expressed as mean±standard deviation or median (interquartile range) as appropriate. Data were first tested for normality by using a one-sample Kolmogorov-Smirnov test. One-way analysis of variance (ANOVA) with post hoc test was used to evaluate the level of significance of the difference in parameters of DCE-MRI among three groups. Receiver operating characteristic curves (ROCs) were performed to assess which parameter showed the best accuracy for diagnosis of the nodules. According to the areas under the ROCs (AUROCs), the optimal cutoff values were determined for nodule diagnosis. Ordinal logistic regression analysis was used to estimate further the predictive value of parameters that showed potential diagnostic efficiency. Spearman correlation coefficients were used to analyze the correlation between parameters and histopathological results. P values less than 0.05 indicated statistical significance.

Results

Nodule growth

Twenty-one rats died due to HCC and related complications (n = 19) such as tumour rupture and poor tolerance to anaesthesia (n = 2). Eventually, 39 rats successfully completed the experiment. DCE-MRI was performed from the 5th week to the 16th week following tumour induction;, nodules were initially observed in the MR images in the sixth week, with increasing number and size of nodules over time. Sixty-two nodules with diameter of 1.2-19.7 mm (measured on tissue specimen) corresponding to histological specimen were selected in the microangiography study. These included 13 RNs, 12 DNs, and 37 HCC. One hundred and forty-three nodules with diameter of 1.3-17.2 mm (measured on tissue specimen) were selected in the DCE-MRI study, including 45 RNs, 61 DNs, and 37 HCC. Among them, nine RNs, five DNs, and 13 HCC were shown by both microangiography and DCE-MRI study.

Microangiography findings

At the 6th week, nodules with portal blood supply were present in the hepatic portography. At the 10th week, nodules with arterial blood supply were observed in the hepatic arteriography. Multiple liver nodules were found, with different sizes and blood supplies (Fig. 2). According to blood supply, nodules were divided into three groups: portal blood supply, arterial blood supply, and mixed blood supply. As the malignant degree of nodules increased, the intranodular portal blood supply decreased and the intranodular arterial blood supply increased (Table 1). The intranodular normal hepatic artery gradually disappeared and replaced by tortuous and dilated abnormal arteries.

DCE-MRI findings

The RE-time curves of nodules were divided into four types: continuous slow rising, slow rise and fall, rapid rise but slow fall, and rapid rise and fall (Table 2 and Supplementary Fig. 1). The RE-time curve for RN rose slowly in 53.3 % (24/45) of the cases, and rose and fell slowly in 26.7 % (12/45). The RE-time curve for DN rose slowly in 44.3 % (27/61) of the cases, and rose rapidly, but fell slowly in 41.0 % (25/61). The RE-time curve of HCC rose rapidly, but fell slowly in 40.5 % (15/37) of the cases, and rose and fell rapidly in 29.7 % (11/37). All of the DCE-MRI parameters increased along with increasing grade of nodule malignancy (Table 3 and Fig. 3). The highest K^{trans} and iAUC values were seen in HCC, followed by DN and RN (all $P < 0.05$). K_{ep} was higher in HCC than DN and RN (both $P < 0.05$), and V_e was higher in HCC than RN ($P < 0.05$). There was a positive correlation between each
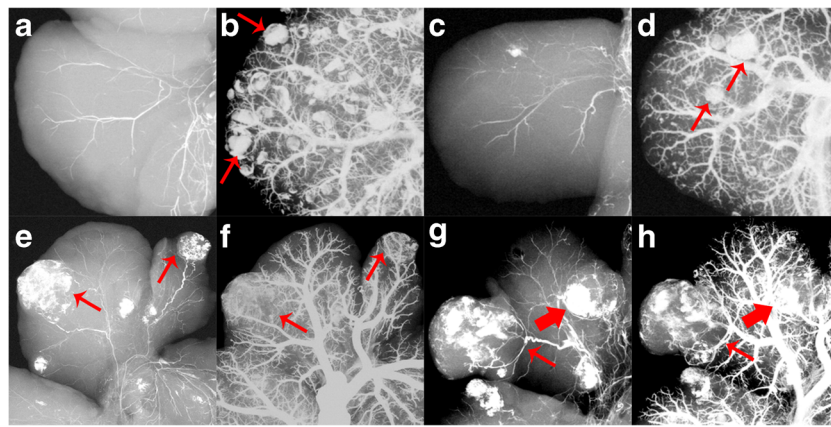
Fig. 2 Microangiography images of nodules in different pathological types. Regenerative nodules all have portal blood supply (**a** and *arrows* in **b**). Dysplastic nodules have portal blood supply (**c** and *arrows* in **d**), mixed blood supply (*thick arrows* in **g** and **h**), or arterial blood supply. HCC has mixed blood supply (*arrows* in **e** and **f**) or arterial blood supply (*thin arrows* in **g** and **h**). Torturous feeding arteries from the hepatic artery are shown on arterial phase in nodules, which have arterial blood supply or mixed blood supply

parameter of DCE-MRI and the pathological classification of liver nodules ($r_{Ktrans} = 0.540$, $r_{Kep} = 0.219$, $r_{Ve} = 0.206$, $r_{iAUC} = 0.521$, all $P < 0.05$). In the diagnosis of DN and HCC, K^{trans} and iAUC had higher AUROC than that of K_{ep} and V_e with high specificity, but low sensitivity (Table 4 and Fig. 4). For HCC diagnosis, K^{trans} and iAUC had higher AUROC than that of K_{ep} and V_e, with both high specificity and high sensitivity (Table 4 and Fig. 4). Ordinal logistic regression analysis showed that K^{trans} was a potential predictive variable for the pathological classification of liver nodules (goodness of fit, 0.970; 95 % confidence intervals, 13.751-24.958). In contrast, iAUC had no predictive value for the pathological classification of liver nodules.

Histopathological and immunohistochemical findings

RNs showed no cellular atypia, but its cell arrangement was random and disorganized with varying amounts of hyperplastic oval cells or a small amount of fibroblasts around the nodules (Fig. 3). The cells in DNs showed different degrees of atypia, increased cellular density and a higher nuclear-cytoplasmic ratio (Fig. 3). The cells in HCC were obviously atypical with enlarged cellular nuclei, distinct nucleolus, and thick nuclear membrane (Fig. 3). Mitoses, necrosis, and haemorrhage were common findings. In some HCC nodules, microvascular invasion and spread of tumour cells to the adjacent parenchyma were seen. CD31 staining showed rare unpaired arteries in RN, a small amount of unpaired arteries in DN and a large amount of unpaired arteries in HCC (Fig. 5), which was consistent with the trend of DCE-MRI parameters.

Discussion

Our experimental study indicated DCE-MRI was a promising method for the non-invasive monitoring of angiogenesis during malignant transformation of hepatocellular nodules in cirrhosis. Among the DCE-MRI parameters, K^{trans} was the most closely related to the pathological classification of liver nodules.

Table 1 Blood supply of different pathological type of nodules in microangiography

Blood supply	Pathological type of the nodules		
	RN	DN	HCC
Portal blood supply	13 (100 %)	3 (25 %)	0
Mixed blood supply	0	5 (41.7 %)	20 (54.1 %)
Arterial blood supply	0	4 (33.3 %)	17 (45.9 %)
Total	13	12	37

RN = regenerative nodule, DN = dysplastic nodule, HCC = hepatocellular carcinoma

Table 2 RE-time curves in different pathological kind of nodules

RE-time curve	Pathological type of the nodules		
	RN	DN	HCC
Constant slow rise	24 (53.3 %)	27 (44.3 %)	6 (16.2 %)
Slow rise and fall	12 (26.7 %)	3 (4.9 %)	5 (13.5 %)
Rapid rise but slow fall	7 (15.6 %)	25 (41.0 %)	15 (40.5 %)
Rapid rise and fall	2 (4.4 %)	6 (9.8 %)	11 (29.7 %)
Total	45	61	37

RN = regenerative nodule, DN = dysplastic nodule, HCC = hepatocellular carcinoma

Table 3 Parameters of DCE-MRI in different pathological type of nodules ($\bar{x} \pm s$)

Group	K^{trans} (min^{-1})	K_{ep} (min^{-1})	V_e	iAUC
RN (n = 45)	0.076 ± 0.022	0.397 ± 0.175	0.250 ± 0.103	6.499 ± 2.032
DN (n = 61)	0.092 ± 0.036[*]	0.400 ± 0.167	0.276 ± 0.110	8.195 ± 3.727[*]
HCC (n = 37)	0.140 ± 0.043[**##]	0.491 ± 0.171[*#]	0.314 ± 0.107[**]	12.632 ± 4.425[**##]
F value	37.597	3.986	3.627	32.719
P value	0.000	0.021	0.029	0.000

Note:Data are mean ± standard deviations.

RN = regenerative nodule DN = dysplastic nodule, HCC = hepatocellular carcinoma

[*] $P < 0.05$, [**] $P < 0.01$ for comparison with RN

[#] $P < 0.05$, [##] $P < 0.01$ for comparison with DN

K^{trans} = transfer constant, K_{ep} = rate constant, V_e = xtravascular extracellular volume fraction; iAUC = initial area under the gadolinium concentration-time curve

As a non-invasive functional MR imaging method, DCE-MRI can show the features of tumour microvascularity with respect to vascular permeability and other physiologic properties. Of the commonly used quantitative parameters, K^{trans} reflects the transport of contrast agent from the blood vessels to extravascular extracellular space (EES) across the endothelial cell membrane, namely the intake of contrast agent [13]. In the majority of tumours including HCC, K^{trans} indicates a

Fig. 3 Imaging findings of different kinds of nodules. Images of T$_2$WI, K^{trans}, relative enhancement-time curve, and haematoxylin-eosin (HE)-stained samples (Original magnification, ×200) of RN, DN, HCC in rats. The images of K^{trans} show the selection of ROIs of the nodules (*yellow circles*). In RE-time curves, the red, green, and yellow curves represent artery input function, vein input function, and the relative enhancement degree of nodule, respectively. The RE-time curve of RN has a constant slow rise, and of DN it rises rapidly, but falls slowly, and the RE-time curve of HCC rises and falls rapidly. HE stain shows that the size and shape of cells in RN are similar to normal liver cells, but its arrangement is random and disorganized. The cells in DN are atypical and with increased cellular density. And the cells in HCC are obviously atypical and necrosis (*arrow*) is more likely to see
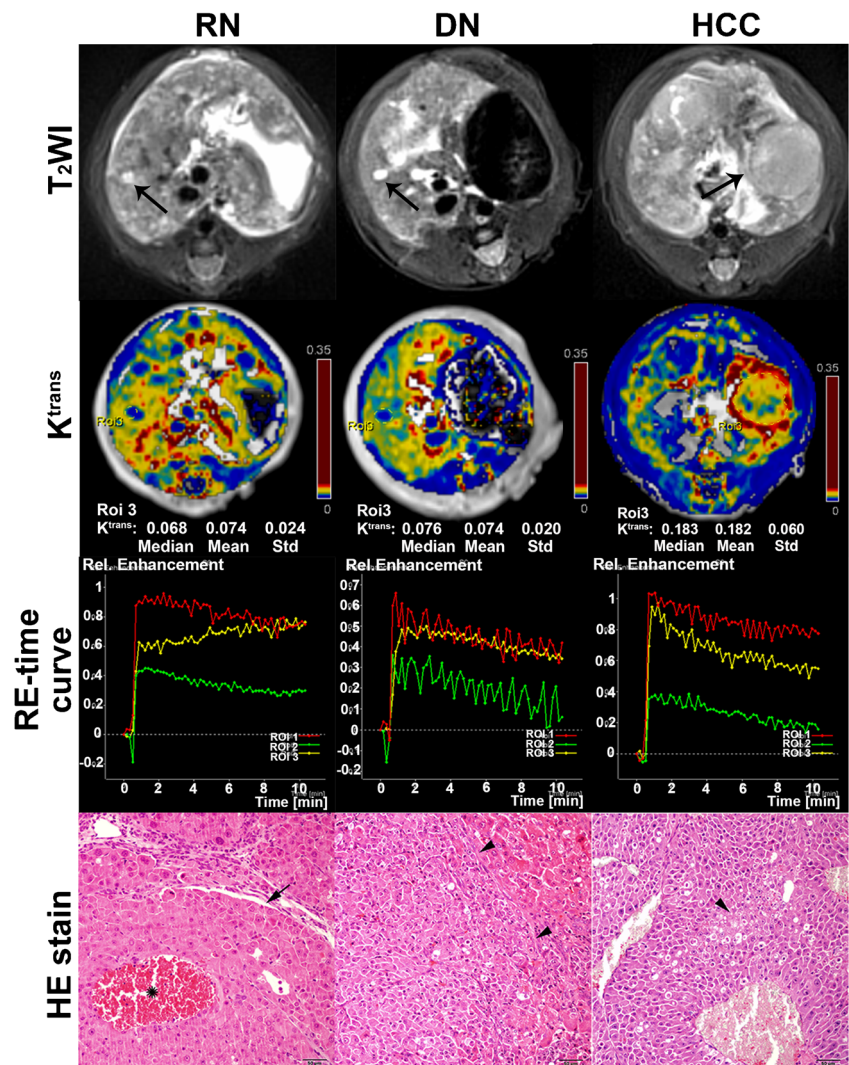
Table 4 Cutoff and performance values of DCE-MRI parameters for diagnosis in rats with cirrhotic nodules

	RN vs DN + HCC				RN + DN vs HCC			
	K^{trans}	K_{ep}	V_e	iAUC	K^{trans}	K_{ep}	V_e	iAUC
Cutoff point	0.104	0.448	0.251	9.765	0.111	0.473	0.251	9.888
AUROC	0.738	0.578	0.599	0.728	0.850	0.664	0.624	0.840
Sensitivity	0.551	0.490	0.633	0.429	0.730	0.622	0.757	0.703
Specificity	0.933	0.756	0.578	1.000	0.821	0.736	0.500	0.858
P value	$P < 0.01$	0.134	0.058	$P < 0.01$	$P < 0.01$	0.003	0.025	$P < 0.01$

RN = regenerative nodule, DN = dysplastic nodule, HCC = hepatocellular carcinoma

K^{trans} = transfer constant, K_{ep} = rate constant, V_e = extravascular extracellular volume fraction; iAUC = initial area under the gadolinium concentration-time curve; AUROC = area under the receiver operating characteristic curve

combination of both flow and permeability properties of the tissue. High K^{trans} values usually reflect both high permeability and high perfusion, and are associated with increased degree of malignancy. In our study, K^{trans} of HCC was significantly higher than those of RN and DN. In 70.3 % of cases, the RE-time curve of HCC either rose rapidly and fell slowly, or rose and fell rapidly. This observation above all indicated that the blood flow and permeability of the nodules increased. In the digital microangiography images we could see the changes of blood vessels visually, and the changes of CD31 staining confirmed the increased tumour blood vessels. In recent years, many studies focus on the application of DCE-MRI on monitoring the efficacy of treatment and estimating prognosis. Zhu et al [31] found significant decreases in K^{trans} and K_{ep} after treatment in advanced hepatocellular carcinoma ($P < 0.0001$). The extent of decrease in K^{trans} was substantially higher in patients who experienced partial response or stable disease compared with that in patients with progressive disease or who died during the first two cycles of therapy. Significant decreases in AUC and K^{trans} were noted in tumours after bevacizumab in the study of Yopp et al [32]. Hsu et al [18]

found that percentage of K^{trans} change (difference between pre- and post-treatment) is an independent predictor of tumour response, progression free survival, and overall survival. These studies supported the results of our study. Our ROC curve analysis showed that K^{trans} had better diagnostic accuracy, while the sensitivity was low when distinguishing DN and HCC from RN. This could be due to the lack of abnormal new blood vessels in some DNs, especially LGDNs, which resulted in a less obvious change of blood supply and vascular permeability. Xu [29] et al reported that due to the reduction in the number of portal veins and normal hepatic arteries, and the shortage of abnormal arteries, the blood flow of DN may be slightly lower than the RN.

IAUC is defined as a measure of the amount of contrast agent delivered to and retained by a tumour in a given time period. IAUC relates to the blood flow in the tumour, the permeability of tumour vessels and the volume of EES of tumour [33, 34]. Similar to K^{trans}, iAUC of HCC was significantly higher than that of RN and DN, and had a relatively large AUROC. However, ordinal logistic regression analysis showed that iAUC had no predictive value for the
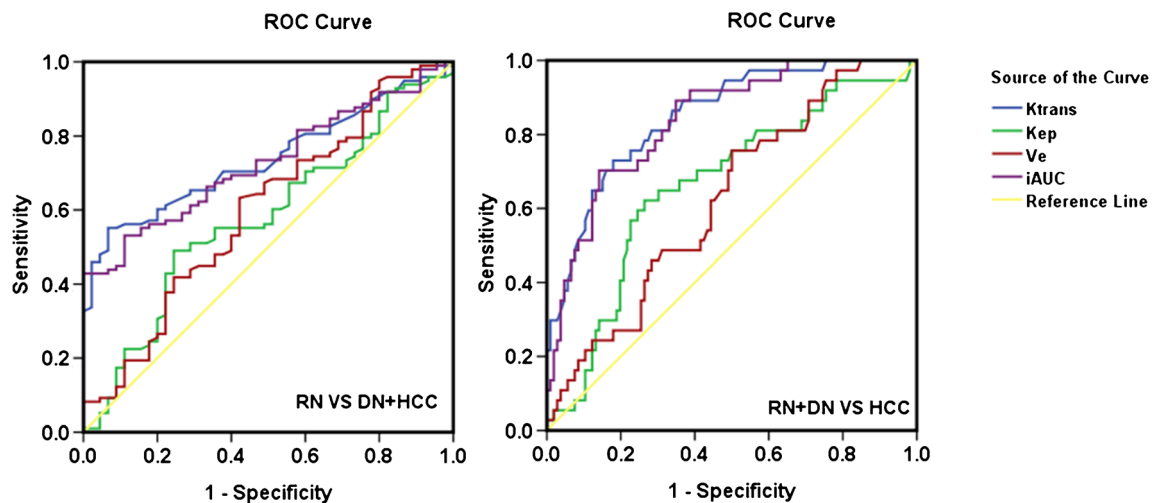

Fig. 4 ROC curves for DCE-MRI parameters for distinguish RN (a) or HCC (b) from cirrhotic nodules. K^{trans} and iAUC have bigger AUROC than that of K_{ep} and V_e both in the diagnosis of DN and more malignant nodules and in the diagnosis of HCC
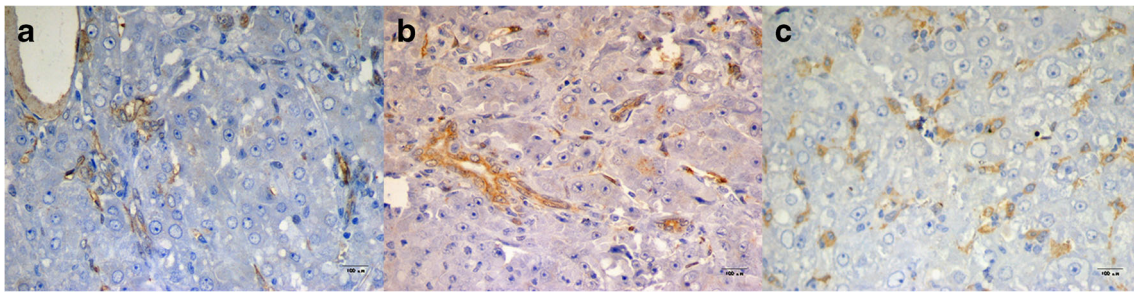
Fig. 5 CD31 staining of RN (**a**), DN (**b**) and HCC (**c**), the numbers of unpaired artery were increased gradually along with increasing grade of malignancy of the nodules

pathological classification of liver nodules. IAUC is a mixed parameter and all the factors above-mentioned such as the blood flow in the tumour, the permeability of tumour vessels and the volume of EES of tumour can affect the iAUC values. It is possible that these factors reduce the diagnostic value of iAUC to some extent.

There were several limitations in our current study. First, we used a two-compartment Tofts model rather than a dual-input two-compartment model. However, the post-processing software (Tissue 4D) had been approved by the US Food and Drug Administration (FDA) for investigating liver perfusion state. Second, although rats were in deep anaesthesia and were wrapped with gauze to restrain their breathing movement, there were still some motion artefacts from breathing movement and intestinal peristalsis, which were difficult to avoid. Third, when nodules were numbered, in spite of the combination of images of axial T_1WI, T_2WI, DCE-MRI and coronal T_2WI, it is possible that some nodules and images did not correspond accurately.

In conclusion, based on our experimental study, DCE-MRI was a promising method for the non-invasive monitoring of angiogenesis during malignant transformation of hepatocellular nodules in cirrhosis. Among the DCE-MRI parameters, the diagnostic accuracy of K^{trans} was the highest. Elevated K^{trans} suggested the transformation of nodules to HCC. Future clinical studies are warranted to validate these initial findings.

References

1. Ferlay J, Shin HR, Bray F, Forman D, Mathers C, Parkin DM (2010) Estimates of worldwide burden of cancer in 2008. Int J Cancer 127:2893–2917
2. Forner A, Llovet JM, Bruix J (2012) Hepatocellular carcinoma. Lancet 379:1245–1255
3. Sherman M (2010) Hepatocellular carcinoma: epidemiology, surveillance, and diagnosis. Semin Liver Dis 30:3–16
4. Alazawi W, Cunningham M, Dearden J, Foster GR (2010) Systematic review: outcome of compensated cirrhosis due to chronic hepatitis C infection. Aliment Pharmacol Ther 32:344–355
5. International Consensus Group for Hepatocellular Neoplasia (2009) Pathologic diagnosis of early hepatocellular carcinoma: a report of the international consensus group for hepatocellular neoplasia. Hepatology 49:658–664
6. Kim YS, Song JS, Lee HK, Han YM (2015) Hypovascular hypointense nodules on hepatobiliary phase without T2 hyperintensity on gadoxetic acid-enhanced MR images in patients with chronic liver disease: long-term outcomes and risk factors for hypervascular transformation. Eur Radiol
7. Song KD, Kim SH, Lim HK, Jung SH, Sohn I, Kim HS (2015) Subcentimeter hypervascular nodule with typical imaging findings of hepatocellular carcinoma in patients with history of hepatocellular carcinoma: natural course on serial gadoxetic acid-enhanced MRI and diffusion-weighted imaging. Eur Radiol 25:2789–2796
8. Tajima T, Honda H, Taguchi K et al (2002) Sequential hemodynamic change in hepatocellular carcinoma and dysplastic nodules: CT angiography and pathologic correlation. AJR Am J Roentgenol 178:885–897
9. Matsui O, Kobayashi S, Sanada J et al (2011) Hepatocelluar nodules in liver cirrhosis: hemodynamic evaluation (angiography-assisted CT) with special reference to multi-step hepatocarcinogenesis. Abdom Imaging 36:264–272
10. Park YN, Yang CP, Fernandez GJ, Cubukcu O, Thung SN, Theise ND (1998) Neoangiogenesis and sinusoidal "capillarization" in dysplastic nodules of the liver. Am J Surg Pathol 22:656–662
11. Hayashi M, Matsui O, Ueda K et al (1999) Correlation between the blood supply and grade of malignancy of hepatocellular nodules associated with liver cirrhosis: evaluation by CT during intraarterial injection of contrast medium. AIR Am J Roentgenol 172:969–976
12. Boss MK, Muradyan N, Thrall DE (2013) DCE-MRI: a review and applications in veterinary oncology. Vet Comp Oncol 11:87–100
13. Tofts PS, Brix G, Buckley DL et al (1999) Estimating kinetic parameters from dynamic contrast-enhanced T(1)-weighted MRI of a diffusable tracer: standardized quantities and symbols. J Magn Reson Imaging 10:223–232

14. Leach MO, Morgan B, Tofts PS et al (2012) Imaging vascular function for early stage clinical trials using dynamic contrast-enhanced magnetic resonance imaging. Eur Radiol 22:1451–1464

15. Türkbey B, Thomasson D, Pang Y, Bernardo M, Choyke PL (2010) The role of dynamic contrast-enhanced MRI in cancer diagnosis and treatment. Diagn Interv Radiol 16:186–192

16. Hötker AM, Mazaheri Y, Zheng J et al (2015) Prostate Cancer: assessing the effects of androgen-deprivation therapy using quantitative diffusion-weighted and dynamic contrast-enhanced MRI. Eur Radiol 25:2665–2672

17. Miyazaki K, Jerome NP, Collins DJ et al (2015) Demonstration of the reproducibility of free-breathing diffusion-weighted MRI and dynamic contrast enhanced MRI in children with solid tumours: a pilot study. Eur Radiol 25:2641–2650

18. Hsu CY, Shen YC, Yu CW et al (2011) Dynamic contrast-enhanced magnetic resonance imaging biomarkers predict survival and response in hepatocellular carcinoma patients treated with sorafenib and metronomic tegafur/uracil. J Hepatol 55:858–865

19. O'Connor JP, Jackson A, Parker GJ et al (2012) Dynamic contrast-enhanced MRI in clinical trials of antivascular therapies. Nat Rev Clin Oncol 9:167–177

20. Barnes SL, Whisenant JG, Loveless ME et al (2012) Practical dynamic contrast enhanced MRI in small animal models of cancer: data acquisition, data analysis, and interpretation. Pharmaceutics 4: 442–478

21. Aryal MP, Nagaraja TN, Keenan KA et al (2014) Dynamic contrast enhanced MRI parameters and tumor cellularity in a rat model of cerebral glioma at 7 T. Magn Reson Med 71:2206–2214

22. Nasui OC, Chan MW, Nathanael G et al (2014) Physiologic characterization of inflammatory arthritis in a rabbit model with BOLD and DCE MRI at 1.5 Tesla. Eur Radiol 24:2766–2778

23. Thukral A, Thomasson DM, Chow CK et al (2007) Inflammatory breast cancer: dynamic contrast-enhanced MR in patients receiving bevacizumab–Initial experience. Radiology 244(3):727–735

24. Mross K, Fasol U, Frost A et al (2009) DCE-MRI assessment of the effect of vandetanib on tumor vasculature in patients with advanced colorectal cancer and liver metastases: a randomized phase I study. J Angiogenes Res 1:5

25. Hahn OM, Yang C, Medved M et al (2008) Dynamic contrast-enhanced magnetic resonance imaging pharmacodynamic biomarker study of sorafenib in metastatic renal carcinoma. J Clin Oncol 26: 4572–4578

26. Alonzi R, Padhani AR, Allen C (2007) Dynamic contrast enhanced MRI in prostate cancer. Eur J Radiol 63:335–350

27. Jarnagin WR, Schwartz LH, Gultekin DH et al (2009) Regional chemotherapy for unresectable primary liver cancer: results of a phase II clinical trial and assessment of DCE-MRI as a biomarker of survival. Ann Oncol 20:1589–1595

28. Hirashima Y, Yamada Y, Tateishi U et al (2012) Pharmacokinetic parameters from 3-Tesla DCE-MRI as surrogate biomarkers of antitumor effects of bevacizumab plus FOLFIRI in colorectal cancer with liver metastasis. Int J Cancer 130:2359–2365

29. Xu H, Xie JX, Li X et al (2008) Perfusion-weighted MRI in evaluating the intranodular hemodynamic characteristics of dysplastic nodules and hepatocellular carcinomas in an experimental rat model. J Magn Reson Imaging 27:102–109

30. Wang H, Van de Putte M, Chen F et al (2008) Murine liver implantation of radiation-induced fibrosarcoma: characterization with MR imaging, microangiography and histopathology. Eur Radiol 18: 1422–1430

31. Zhu AX, Sahani DV, Duda DG et al (2009) Efficacy, safety, and potential biomarkers of sunitinib monotherapy in advanced hepatocellular carcinoma: a phase II study. J Clin Oncol 27:3027–3035

32. Yopp AC, Schwartz LH, Kemeny N et al (2011) Antiangiogenic therapy for primary liver cancer: correlation of changes in dynamic contrast-enhanced magnetic resonance imaging with tissue hypoxia markers and clinical response. Ann Surg Oncol 18:2192–2199

33. Walker-Samuel S, Leach MO, Collins DJ (2006) Evaluation of response to treatment using DCE-MRI: the relationship between initial area under the gadolinium curve (IAUGC) and quantitative pharmacokinetic analysis. Phys Med Biol 51:3593–3602

34. Koh TS, Thng CH, Hartono S et al (2011) A comparative study of dynamic contrast-enhanced MRI parameters as biomarkers for anti-angiogenic drug therapy. NMR Biomed 24:1169–1180